NASA TECHNICAL NOTE

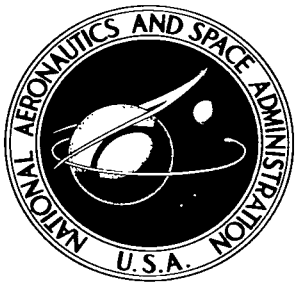

NASA TN D-2087

NASA TN D-2087

EFFECT OF AMBIENT AIR VELOCITY ON ATOMIZATION OF TWO IMPINGING WATER JETS

by David A. Bittker

Lewis Research Center
Cleveland, Ohio

NATIONAL AERONAUTICS AND SPACE ADMINISTRATION • WASHINGTON, D. C. • FEBRUARY 1964

EFFECT OF AMBIENT AIR VELOCITY ON ATOMIZATION OF TWO IMPINGING WATER JETS

By David A. Bittker

Lewis Research Center
Cleveland, Ohio

NATIONAL AERONAUTICS AND SPACE ADMINISTRATION

For sale by the Office of Technical Services, Department of Commerce,
Washington, D.C. 20230 -- Price $1.00

EFFECT OF AMBIENT AIR VELOCITY ON ATOMIZATION OF TWO IMPINGING WATER JETS

SUMMARY

Drop-size distributions were measured for the sprays formed by two 0.089-inch-diameter impinging water jets. Jet impingement angles of 30°, 60°, and 90° and jet velocities of 30, 60, and 74 feet per second were used. These variables were held constant, while the primary variable of this work (i.e., the difference between the ambient air velocity and the liquid jet velocity) was changed from 0 to 120 feet per second.

All distributions show bimodal characteristics with number-median diameters of approximately 200 and 500 microns for the two modes. For low jet velocities, increasing the velocity difference decreases the mass-median diameter of the large-diameter mode and increases the percentages of mass and drops in the small-diameter mode. In the range of velocity difference 0 to 120 feet per second, the volume-number-mean and mass-median diameters of the complete spray decrease as velocity difference increases, except for the highest jet velocity.

INTRODUCTION

The process of liquid atomization by rocket engine injectors is dependent on several experimental variables, and the functional relations are not fully understood. Inasmuch as the whole combustion process is exceedingly complicated, some pertinent information can be obtained by first studying atomization by a single injector element in cold flow. This technique was used in the investigation of reference 1 to study the drop-size distribution of the water spray formed by a single pair of impinging jets. The impingement angle was the variable of interest in that work, the results of which showed that the spray is better atomized as the injector angle increases.

The current study is a continuation of the work described in reference 1. Drop-size distributions for the injectors used in reference 1 were obtained to study the effect of changing only the difference between the ambient air velocity and the water jet velocity. The most extensive data were taken for a 60° impingement angle, but angles of 30° and 90° were also used in some experiments. Drop-size data were obtained from measurements of shadowgraph pictures taken 8 inches or more downstream of the impingement point in a duct connected to an exhaust system. The drops were sized and counted by an electronic particle analyzer.

The values of jet angle, jet velocity, velocity difference, airflow, and Reynolds number were selected to cover the ranges typical of rocket combustors. As in reference 1, the data could be fitted by assuming a bimodal size distribution. The properties of each mode as well as the properties of the complete distributions are shown. The effect of velocity difference is presented at three jet velocities.

EXPERIMENTAL APPARATUS AND PROCEDURE

Apparatus

The experimental setup used in this work is shown in figures 1 and 2 and described in detail in reference 1. Figure 1 shows the impinging-jet atomizer and figure 2(a) the complete apparatus, consisting of an atomizer mounted in a 4- by 12-inch duct, an optical system, and a camera. Figure 2(b) shows a schematic view of the optical system and indicates the sampling position. An improved light source was used in this study, which enabled the exposure time for each picture to be shortened to 1/2 microsecond from the value of 1-microsecond used in reference 1. The light-source diameter was 0.015 inch. The centerline of the optical path was perpendicular to the principal plane of the spray at its axis of symmetry (the horizontal plane of the impinging jets). A study of the spatial characteristics of impinging-jet sprays reported in reference 2 showed that such an alinement gives a representative sample for determining drop-size distribution. The photographs obtained had a 1-to-1 magnification ratio.

The sample size measured for each experimental condition, in all but three cases, was larger than 9000 drops. A check was made of each spray to verify that the final distribution measured did not change with sample size. The expected statistical accuracy was also estimated by using the work of reference 3 (which is also to be published as part of a Ph.D. thesis) to calculate the width of the 95 percent confidence band for the range of sample sizes obtained. The calculations for two sample sizes are summarized in the following table:

Fraction of drops in size group	Number of drops in distribution, N	
	10,000	4000
	Range of values of fraction of drops expected with 95 percent confidence	
0.05	0.05±0.004	0.05±0.006
.10	.10±0.006	.10±0.009
.15	.15±0.007	.15±0.011
.20	.20±0.008	.20±0.012
.25	.25±0.009	.25±0.013

This table shows that the statistical error is no greater than 12 percent, even for the smaller sample size, when as little as 5 percent of the total sample is counted. The error is obviously increased when less than 5 percent of the total sample is read. The error magnitude cannot be stated quantitatively; however,

it will be seen that less weight was given to these thinly populated size groups than to the more populous ones when the data were analyzed.

The various test conditions used in this study are given in table I.

Drop-Size Analysis Procedure

The spray photographs were measured in the electronic particle analyzer described in references 4 and 5. Particles in the size range from 200 to 6400 microns can be counted by this device with the 1-to-1 magnification used in the photography. This range is divided into 10 steps, for which the ratio of the upper to the lower size limit in a step is always $\sqrt{2}$. The digital counter on the analyzer shows the number of drops larger than a preselected size. The number of drops in each size group is found by differences in the several counts. The accuracy of the particle analyzer is estimated to be ±10 percent in counting drops in the smallest size range (200 to 280μ) and to be ±3 percent for the other size ranges.

RESULTS AND DISCUSSION

Analysis of Distributions

Experimental data. - The initial plan called for all sprays to be photographed at the same distance downstream of the impingement point; however, photographs for all desired conditions could not be obtained at the distance first planned, namely, 8 inches. With the 30° angle injector, the liquid sheet formed by the jet impingement was not completely broken up into drops 8 inches downstream. With the 90° angle injector, the spray hit the walls of the duct at low velocity differences, and thus no photographs of the spray could be taken below Δv = 37 feet per second. (Symbols are defined in appendix A.) In several experiments, it was determined that the drop-size distribution of a given spray changes significantly with distance from the impingement point, even after the liquid sheet is disintegrated. It is therefore impossible to compare data at different downstream distances. The change in two drop-size distributions with distance is shown for the 60° injector in the following table, which shows the percentage of drops in each size group for the same spray photographed 8 and 16 inches downstream of the impingement point.

Average diameter of size group, D_{av}, μ	Jet velocity, v_j, ft/sec			
	30		74	
	Velocity difference, Δv, ft/sec			
	60		120	
	Downstream distance, in.			
	8	16	8	16
	Percentage of drops in size group (60° angle injector)			
242	28.51	41.00	44.10	58.76
341	24.71	24.12	25.13	25.59
484	18.53	16.17	15.05	10.43
682	16.38	12.30	10.15	4.21
965	8.06	5.07	4.18	.89
1365	2.90	1.16	1.10	0.12
1930	.77	.18	.26	0
2720	.13	0	.03	0
3860	.01	0	0	0

The distributions measured with the 30° angle injector had to be photographed 16 inches downstream of the impingement point, so these data cannot be compared quantitatively with data from the other injectors, which were photographed 8 inches downstream. Qualitative conclusions, however, were obtained by comparing the trends in the two sets of data.

Some typical spray photographs are shown in figure 3. All pictures in figure 3(a) were taken 8 inches downstream of the 60° angle injector. Figure 3(b) shows sprays from the 30° angle injector taken at distances of 8 and 16 inches; the pictures taken at 8 inches illustrate a spray that has not formed drops.

Drop-count data obtained with the electronic particle analyzer are listed in table II for all conditions used. Although a large number of drops that were less than 200 microns in diameter existed in each spray, these drops were neither counted nor included in table II. From direct measurements on enlarged prints of several spray photographs, it was estimated that approximately 40 percent of the drops were usually not counted.

Some typical number-size distributions are shown in figure 4. The logarithm of ΔN, the number of drops in a size group, is plotted as a function of the logarithm of the mean diameter of the size group. These distribution curves, which are for a sample size at least 10 times greater than those in reference 1, show the same inflection points as those of the previous work. It was therefore assumed that all distributions are composed of the sum of two individual logarithmic normal distributions, that is, that they are bimodal. Reference 1

reports other instances of bimodal and multimodal distributions, and reference 6 lends support to the idea that the drop-size distribution from an impinging-jet injector should be bimodal.

Figure 4(a) shows the two logarithmic normal modes into which the distribution can be separated by the technique outlined in the following section. The curve in figure 4(a) is typical of the fit that was obtained for all but two of the distributions measured. The distribution shown was obtained with the 60° angle injector at a jet velocity of 60 feet per second. When the same injector was used at a jet velocity of 30 feet per second for velocity differences of 0 and 30 feet per second, distribution curves with an abnormally high percentage of large-diameter drops were obtained. One of these two curves is shown in figure 4(b).

Selection of modes. - In the previous work (ref. 1), the separation of the experimental distribution into two logarithmic normal modes was done graphically. In the present work the separation into modes was done analytically with the aid of an IBM 7090 digital computer. It is shown in appendix B that a logarithmic normal distribution plots as a parabola on log-log paper (see eq. (B3)). This fact was used as follows to obtain two modes for each distribution. Several data points at the large-diameter end of the distribution were assumed to belong entirely to the large-diameter mode, which will be called mode 2. These points were then fitted to a parabola by the weighted least-squares method of reference 7. The weighting factor takes into account the fact that the expected experimental error of a given measurement decreases as the number of particles counted for the measurement increases.

When, after several tries, an apparently satisfactory mode 2 curve was obtained, two or three points on the mode 1 curve could be obtained for the intermediate size groups. Attempts were then made to fit a parabola through these points by the ordinary least-squares method. If a satisfactory fit was not obtained for mode 1 after a few attempts, mode 2 was refitted with a different maximum point for the parabola, and then mode 1 was refitted with the new mode 2. In this manner, the constant B_i's of equation (B3) were obtained for each mode.

The entire curve-fitting process requires a certain amount of judgment because of the difficulty in selecting the peaks of the parabolas at the beginning of the routine, especially for mode 1. With experience, these maximums could be estimated within narrow limits by the mathematical curve-fitting technique. No claim is made, however, that the modes shown are the only ones into which the experimental distributions can be separated.

Calculation of spray properties. - After a particular bimodal distribution has been built up by the technique just described, properties of the new distribution can be calculated. The following properties of each individual mode were calculated:

(1) Number-median diameter D_{N_i}: For the symmetric logarithmic-normal distribution D_{N_i} is the value for which the parabolic distribution curve has its maximum. (See the dashed curves of fig. 4.)

(2) Geometric mean deviation σ_i: This deviation is a measure of the spread of the distribution curve and is given, for a logarithmic-normal parabola, by

$$\sigma_i = \frac{\mathscr{D}_i}{D_{N_i}} \tag{1}$$

where $\mathscr{D}_i$ is the diameter for which 84.13 percent of the drops in the distribution have a smaller size. This quantity was evaluated by drawing a horizontal line across the parabolic curve at an ordinate value equal to 0.6067 times the maximum height of the parabola. The abscissa value at which this line intersects the right half of the parabola is $\mathscr{D}_i$.

(3) Mass-median diameter D_{M_i}: For the logarithmic-normal modes D_{M_i} was calculated by use of the equation given in reference 8

$$\frac{D_{M_i}}{D_{N_i}} = e^{3(\ln \sigma_i)^2} \tag{2}$$

(4) Total number of drops in each mode N_i: This number was calculated from equation (B4a), where the values of B_0, B_1, and B_2 are those obtained by the parabolic curve-fitting procedure described in the previous section.

(5) Total mass in each mode M_i: The total mass was calculated from the following equation:

$$M_i = \sum_j (\Delta N)_j (D_{av})_j^3 \tag{3}$$

where $(D_{av})_j$ is the average diameter of experimental size group j and $(\Delta N)_j$ is the number of drops in that size group, as determined from equation (B3).

In addition to these mode properties, the following average diameters of the complete bimodal distribution were calculated:

(1) Mass-median diameter D_T: This diameter was determined by directly summing the mass contributions for each mode and plotting percent of total spray mass contained in drops with diameters less than or equal to D_{av} as a function of D_{av}.

(2) Volume-number-mean diameter D_{30}: This diameter was calculated from equations (C8) and (C9) of appendix C, with the previously calculated values of N_1, N_2, D_{M_i}, and σ_i for each mode.

Properties of Individual Modes

Median diameters. - Neither the number-median nor the mass-median diameter of mode 1 shows any trend in magnitude with jet angle, jet velocity, or velocity

difference for the data taken 8 inches downstream of the inpingement point. This is shown by the data in table II for jet angles of 60° and 90°. (See appendix D for a discussion of an alternate curve-fitting procedure for these experiments, which assumes constant average values of D_{N_1} and D_{M_1}.) Although the number-median diameters for the 30° angle injector agree with the other data, the values of the geometric mean deviation, and thus the mass-median diameter, are generally larger than values for the other data. The mass-median diameter data for the 30° injector are somewhat scattered; however, there does not seem to be any significant trend of this quantity with jet velocity or velocity difference.

Figure 5 shows the effect of velocity difference on the number-median diameter of mode 2. For this and the other spray properties, three comparison plots are presented in the figure: (1) a plot of the 60° angle injector data as a function of velocity difference for three values of jet velocity (fig. 5(a)), (2) a plot of the 30° angle injector data as a function of velocity difference for two values of jet velocity (fig. 5(b)), and (3) a plot of the 90° and the 60° angle injector data as a function of velocity difference for the same value of jet velocity. Data points from reference 1 have been placed on the curves for comparison purposes only. In figure 5(a), it can be seen that there is little effect of velocity difference on the number median. There is an indication, however, that this diameter decreases slightly when the velocity difference is increased above 60 feet per second at the lowest jet velocity. The effect of velocity difference is more noticeable for the 30° angle injector (fig. 5(b)). For the lower jet velocity the number median decreases with increasing velocity difference. This trend is less apparent at the higher jet velocity. Increasing the injector angle from 60° to 90° has no effect on the number median, as shown in figure 5(c) for the 30-foot-per-second jet velocity.

The effect of velocity difference on the mass-median diameter of mode 2 is somewhat more significant than its effect on the number median (fig. 6). For both the 30° and the 60° angle injectors the decrease in mass-median diameter with increasing velocity difference is most noticeable at the lowest jet velocity and practically disappears as the jet velocity reaches 74 feet per second. In figure 6(c) it can be seen that velocity difference has about the same effect on the mass-median diameter for the two injectors used; however, the actual values are lower for the better atomizing 90° injector than they are for the 60° injector. Figures 6(a) and (b) show that increasing the jet velocity at constant Δv generally decreases the mass-median diameter of mode 2. The effect is greatest at $\Delta v = 0$ and decreases steadily with increasing velocity difference.

Number and mass percentages in each mode. - Another measure of the degree of atomization is the distribution of drops and spray mass between the two modes. The effect of velocity difference on the percentage of drops in mode 1 is shown in figure 7. For both the 30° and the 60° angle injectors this percentage increases steadily at all jet velocities. The effect that velocity difference has on this number percentage disappears when the jet angle is increased from 60° to 90° at the 30-foot-per-second jet velocity (fig. 7(c)). The data in figures 7(a) shows that increasing the jet velocity at a fixed velocity difference increases the percentage of drops in mode 1. The data of figure 7(b) are too scattered to show any trend with jet velocity.

Figure 8 shows the effect of velocity difference on the percentage of mass in mode 1. In figures 8(a) and (b), the beneficial effect of velocity difference on the atomization is about the same at all jet velocities. Figure 8(a) shows that increasing jet velocity aids the atomization for a given velocity difference, but the data of figure 8(b) are too scattered to show any effect of jet velocity on the mode-1 mass percentage for this injector. The effect of changing jet angle from 60° to 90° (fig. 8(c)) is simply to displace the mass percentage curve upward in going to the better atomizing 90° angle injector.

ATOMIZATION OF COMPLETE SPRAY

Volume-Number-Mean Diameter

Figure 9 shows that increasing the velocity difference decreases the volume-number-mean diameter for all three injectors. This improvement in atomization is greatest at the lowest jet velocity and disappears at the highest jet velocity, as shown by the data for both the 60° and the 30° injectors (figs. 9(a) and (b)). Figure 9(c) shows that velocity difference has approximately the same effect on the atomization for the 90° angle injector as for the poorer atomizing 60° angle injector. An increase in jet velocity only is seen to improve atomization at lower values of velocity difference for the 30° and 60° angle injectors (figs. 9(a) and (b)). This effect decreased steadily as velocity difference increased.

Mass-Median Diameter

Basically the same trends found for the volume-number-mean are found for the mass median of the complete spray, as shown in figure 10. There is a very sharp decrease in diameter with increasing velocity difference for the lowest jet velocity; however, this trend is gone at the highest jet velocity for both the 60° and the 30° injectors. Figure 10(c) shows that changing jet angles from 60° to 90° gives a slightly more pronounced effect for mass median than that found for volume-number mean. The mass-median diameter, like the volume-number-mean diameter, is decreased by an increase in jet velocity at constant velocity difference.

CONCLUDING REMARKS

Although the actual drop-size distributions obtained in this cold flow study probably would not be found in rocket combustors, the variations in distribution properties should be similar. An important result of this study is the observation that, for an injector with at least 60° impingement angle, atomization is not significantly enhanced by an increase in the velocity difference up to 120 feet per second when the jet velocity is greater than 60 feet per second. The atomization of a 30° angle injector is not improved by velocity difference when the jet velocity is at least 74 feet per second. For these high jet velocities aerodynamic forces do not aid breakup in the range of low velocity difference used in this work. These forces help at lower velocity differences only when a low liquid-jet velocity or jet angle is used; however, increas-

ing the jet velocity at constant velocity difference contributed significantly to improving atomization in many cases.

The limited range of experimental conditions used in this work was not enough to elucidate the mechanism of breakup and the reason for the bimodal distributions. Distributions need to be measured at several points farther downstream from the impingement point to make sure that an equilibrium distribution is obtained. There is a slight possibility that a third mode may be present in the distribution shown in figure 4(b). A much more extensive investigation would have to be undertaken to discover the mechanism of breakup for these impinging-jet injectors.

SUMMARY OF RESULTS

Drop-size distributions were measured in the spray from a pair of 0.089-inch-diameter impinging jets of water. The variable of major interest was the velocity difference between the ambient airflow and the liquid jet. Jet velocity and jet angle were also changed. The following results were obtained:

1. The drop-size distributions could, in every case, be fitted by two logarithmic normal distribution modes.

2. For the lowest jet velocity used (30 ft/sec), atomization of the spray improved steadily as velocity difference was increased from 0 to 120 feet per second for all three injectors.

3. For the highest jet velocity used (74 ft/sec) there was no longer any improvement in atomization due to increasing the velocity difference for either the 30° or the 60° angle injector.

4. For the 30° and the 60° angle injectors, increasing the jet velocity at constant velocity difference improved atomization. The magnitude of the improvement is largest near a velocity difference of zero. For the volume-number-mean and the mass-median diameters of the complete spray, the effect decreased steadily with increasing velocity difference.

Lewis Research Center
National Aeronautics and Space Administration
Cleveland, Ohio, September, 14, 1963

APPENDIX A

SYMBOLS

B_0, B_1, B_2	constants in eq. (B3), defined by eqs. (B4)
D_{av}	average diameter of size group, μ
D_i	volume-number-mean diameter of logarithmic normal mode i, μ
D_M	mass-median diameter for logarithmic normal distribution, μ
D_N	number-median diameter for logarithmic normal distribution, μ
D_T	mass-median diameter of complete distribution, μ
D_{30}	volume-number-mean diameter of bimodal distribution, μ
$\mathscr{D}$	diameter for which 84.13 percent of drops in distribution have a smaller size, μ
M	total mass in distribution
N	number of drops in distribution
ΔN	number of drops in particular size group having average diameter D_{av}
V	volume of drops in distribution
Δv	velocity difference between ambient air and liquid jet, ft/sec
v_j	jet velocity, ft/sec
α	number ratio of mode 1 to mode 2, N_1/N_2
σ	geometric mean deviation of logarithmic normal distribution

Subscript:

i	logarithmic normal mode i

APPENDIX B

MATHEMATICAL EXPRESSION FOR LOGARITHMIC NORMAL DISTRIBUTION

A logarithmic-normal distribution function can be written

$$\frac{\Delta N}{\Delta(\ln D_{av})} = \frac{N_i}{\sqrt{2\pi}\ \ln \sigma_i} \exp\left[\frac{-\left(\ln D_{av} - \ln D_{N_i}\right)^2}{2(\ln \sigma_i)^2}\right] \tag{B1}$$

When the logarithm of this equation is taken, the result is

$$\ln \frac{\Delta N}{\Delta(\ln D_{av})} = A_0 + A_1(\ln D_{av}) + A_2(\ln D_{av})^2 \tag{B2}$$

where A_0, A_1 and A_2 are functions of D_{N_i}, σ_i, N_i. Thus the plot of $\ln \frac{\Delta N}{\Delta(\ln D_{av})}$ as a function of $\ln D_{av}$ will always be a parabola. If equation (B2) is written in the form

$$\ln \Delta N = A_0 + \ln\left[\Delta(\ln D_{av})\right] + A_1(\ln D_{av}) + A_2(\ln D_{av})^2$$

and it is noted that $\Delta(\ln D_{av})$ has a constant value for the size groups used in this work, it is evident that the plot of $\ln \Delta N$ itself as a function of $\ln D_{av}$ is a parabola. Thus, the equation for ΔN as a function of $\ln D_{av}$ is

$$\Delta N = \exp\left[B_0 + B_1 \ln D_{av} + B_2(\ln D_{av})^2\right] \tag{B3}$$

where

$$B_0 = A_0 + \ln\left[\Delta(\ln D_{av})\right] = \ln\left[\frac{N_i}{\sqrt{2\pi}\ \ln \sigma_i}\right] - \frac{1}{2}\left[\frac{\ln D_{N_i}}{\ln \sigma_i}\right]^2 + \ln\left[\Delta(\ln D_{av})\right] \tag{B4a}$$

$$B_1 = A_1 = \frac{\ln D_{N_i}}{(\ln \sigma_i)^2} \tag{B4b}$$

$$B_2 = A_2 = -\frac{1}{2(\ln \sigma_i)^2} \tag{B4c}$$

APPENDIX C

CALCULATION OF VOLUME-NUMBER MEAN DIAMETER OF A BIMODAL DISTRIBUTION

The general expression for the volume-number-mean diameter of a drop-size distribution is

$$D_{30} = \sqrt[3]{\frac{6}{\pi}\frac{V}{N}} \tag{C1}$$

where V is the total volume of the spray and N is the total number of drops in the spray. If, for a bimodal distribution, subscripts 1 and 2 refer to the two modes, the volume-number-mean diameters D_1 and D_2 of the two modes can be written as follows:

$$D_1 = \sqrt[3]{\frac{6}{\pi}\frac{V_1}{N_1}} \tag{C2}$$

$$D_2 = \sqrt[3]{\frac{6}{\pi}\frac{V_2}{N_2}} \tag{C3}$$

Dividing equation (C2) by equation (C3) results in

$$\left(\frac{D_1}{D_2}\right)^3 = \frac{V_1}{N_1}\frac{N_2}{V_2} \tag{C4}$$

If K is substituted for $(D_1/D_2)^3$, equation (C4) can be written in two different ways: first,

$$\frac{V_1}{V_2} = K\frac{N_1}{N_2}$$

which can be written as

$$\frac{V_1 + V_2}{V_2} = \frac{KN_1 + N_2}{N_2} \tag{C5a}$$

and, second,

$$\frac{N_1}{N_2} = \frac{1}{K}\frac{V_1}{V_2}$$

which can be written as

$$\frac{N_1 + N_2}{N_2} = \frac{V_1 + KV_2}{KV_2} \tag{C5b}$$

Dividing equation (C5a) by equation (C5b) gives

$$\frac{N_2}{V_2}\left(\frac{V_1 + V_2}{N_1 + N_2}\right) = K\left(\frac{K\,\frac{N_1}{N_2} + 1}{K + \frac{V_1}{V_2}}\right) \tag{C6}$$

Since $V = V_1 + V_2$ and $N = N_1 + N_2$, equation (C6) becomes

$$\left(\frac{D_{30}}{D_2}\right)^3 = \frac{K\,\frac{N_1}{N_2} + 1}{1 + \frac{N_1}{N_2}} \tag{C7}$$

If the number ratio N_1/N_2 is defined as α and $K = (D_1/D_2)^3$ is substituted, the final result is

$$D_{30}^3 = \frac{D_1^3\alpha + D_2^3}{1 + \alpha} \tag{C8}$$

from which D_{30} can be calculated when only the number ratio for the two modes and the volume-number-mean diameter of each mode are known. These latter volume-number means can be calculated by using the equation given in reference 8

$$D_i = D_{M_i} \exp\left[-\frac{3}{2}(\ln \sigma_i)^2\right] \tag{C9}$$

where D_{M_i} is the mass-median diameter of the mode in question.

APPENDIX D

ALTERNATE CURVE-FITTING PROCEDURE

FOR CERTAIN EXPERIMENTS

It has been stated that the mode-1 number-median diameter and geometric mean deviation are essentially constant for all experiments performed at 8 inches downstream with the 60° and 90° angle injectors. The bimodal curve fitting for these experiments can then be redone by using constant average values for these properties, and the same results for the other mode properties and the complete spray properties should be obtained. This procedure was followed for the 16 experiments performed with the 60° and 90° injectors at the 8-inch downstream distance. New guesses for mode 2 were tried in each case, but only in two experiments did mode 2 change slightly from the curve originally obtained.

The new curves obtained for mode 1 were, in many cases, noticeably different from the old curves, and, of course, did not fit the experimental data as well as the latter had; however, the number and mass percentages in each mode as well as the volume-number-mean and mass-median diameters of the complete distribution agreed within ±12 percent with the values previously obtained. Moreover, the trends of these properties with velocity difference were the same as those previously found. In fact, the scatter of the data points was reduced in certain cases.

REFERENCES

1. Heidmann, Marcus F., and Foster, Hampton H.: Effect of Impingement Angle on Drop-Size Distribution and Spray Pattern of Two Impinging Jets. NASA TN D-872, 1961.

2. Foster, Hampton H., and Heidmann, Marcus F.: Spatial Characteristics of Water Spray Formed by Two Impinging Jets at Several Jet Velocities in Quiescent Air. NASA TN D-301, 1960.

3. Rice, Edward, and Groeneweg, John: Refinements of a Fluorescent Technique for Determining Drop-Size distribution in Liquid Sprays. Univ. Wisconsin, Dec. 1960.

4. Heidmann, Marcus F.: Photography and Analysis of Time Variation in Drop-Size Distribution of a Liquid Spray. Proc. of Fifth Int. Cong. on High Speed Photography, 1960, pp. 519-524.

5. Dell, H. A., Hobbs, D. S., and Richards, M. S.: An Automatic Particle Counter and Sizer. Phillips Tech. Rev., vol. 21, no. 9, Aug. 1960, pp. 253-267.

6. Lewis, J. D.: Studies of Atomization and Injection Processes in the Liquid Propellant Rocket Engine. Paper Presented at Fifth AGARD Combustion and Prop. Colloquium, Braunschweig, Germany, Apr. 9-13, 1962.

7. Kottler, F.: The Distribution of Particle Sizes. Pt. II. The Probability Graphs. Jour. Franklin Inst., vol. 250, no. 5, Nov. 1950, pp. 419-442.

8. Bevans, Rowland S.: Mathematical Expressions for Drop-Size Distributions in Sprays. Conf. on Fuel Sprays, Univ. Michigan, Mar. 30-31, 1949.

TABLE I. - EXPERIMENTAL TEST CONDITIONS

Jet angle, deg	Jet velocity, v_j, ft/sec	Velocity difference, Δv, ft/sec
[a]30	30	0 30 60 120
	74	0 30 60 120
[b]60	30	0 30 60 120
	60	-30 0 30 60 120
	74	0 30 60 120
[b]90	30	37 60 120

[a]Downstream distance, 16 in.

[b]Downstream distance, 8 in.

TABLE II. - DROP COUNTS OBTAINED WITH PARTICLE ANALYZER

AND PROPERTIES OF DROP-SIZE DISTRIBUTIONS

(a) Jet angle, 30°; jet velocity, 30 feet per second; downstream distance, 16 inches

Experimental drop counts				
Average diameter of size group, D_{av}, μ	Velocity difference, Δv, ft/sec			
	0	30	60	120
	Number of drops, ΔN			
242	1065	2751	879	4716
341	817	1977	714	1925
484	764	1545	631	1055
682	947	1480	677	752
965	969	1010	525	403
1365	939	579	379	179
1930	637	180	166	57
2720	310	39	54	22
3860	103	2	4	2
Total	6580	9563	4029	9111
Properties of distributions				
Number-median diameter of mode 1, D_{N_1}, μ	180	190	200	160
Mass-median diameter of mode 1, D_{M_1}, μ	443	623	657	249
Number-median diameter of mode 2, D_{N_2}, μ	1000	800	850	450
Mass-median diameter of mode 2, D_{M_2}, μ	3260	1443	1700	1312
Percentage of drops in mode 1	48.9	77.4	66.5	83.0
Percentage of mass in mode 1	0.5	9.5	4.9	8.2
Volume-number-mean diameter of complete distribution, D_{30}, μ	1446	678	850	438
Mass-median diameter of complete distribution, D_T, μ	2175	1235	1530	1180

TABLE II. - Continued. DROP COUNTS OBTAINED WITH PARTICLE ANALYZER AND PROPERTIES OF DROP-SIZE DISTRIBUTIONS

(b) Jet angle, 30°; jet velocity, 74 feet per second; downstream distance, 16 inches

Experimental drop counts				
Average diameter of size group, D_{av}, μ	Velocity difference, Δv, ft/sec			
	0	30	60	120
	Number of drops, ΔN			
242	3533	2968	4585	3741
341	2706	2426	3537	2048
484	2234	2021	2555	1117
682	2051	1906	2018	791
965	1179	986	1073	335
1365	477	485	466	120
1930	161	143	130	36
2720	29	39	20	12
3860	1	4	0	0
Total	12,371	10,978	14,384	8200
Properties of distributions				
Number-median diameter of mode 1, D_{N_1}, μ	190	180	190	180
Mass-median diameter of mode 1, D_{M_1}, μ	430	336	327	289
Number-median diameter of mode 2, D_{N_2}, μ	620	550	540	430
Mass-median diameter of mode 2, D_{M_2}, μ	1220	1405	1245	1203
Percentage of drops in mode 1	66.8	56.6	63.1	74.8
Percentage of mass in mode 1	6.6	2.8	4.6	8.9
Volume-number-mean diameter of complete distribution, D_{30}, μ	617	672	597	468
Mass-median diameter of complete distribution, D_T, μ	1095	1185	1025	940

TABLE II. - Continued. DROP COUNTS OBTAINED WITH PARTICLE ANALYZER AND PROPERTIES OF DROP-SIZE DISTRIBUTIONS

(c) Jet angle, 60°; jet velocity, 30 feet per second; downstream distance 8 inches

Experimental drop counts				
Average diameter of size group, D_{av}, μ	Velocity difference, Δv, ft/sec			
	0	30	60	120
	Number of drops, ΔN			
242	3318	3925	4284	8372
341	2647	3018	3713	4912
484	2252	2385	2785	3153
682	2364	2242	2461	2127
965	1495	1294	1211	876
1365	736	615	436	322
1930	402	267	115	70
2720	196	96	20	12
3860	55	21	1	1
Total	13,474	13,863	15,026	19,845
Properties of distributions				
Number-median diameter of mode 1, D_{N_1}, μ	170	160	190	160
Mass-median diameter of mode 1, D_{M_1}, μ	291	293	344	269
Number-median diameter of mode 2, D_{N_2}, μ	540	500	500	400
Mass-median diameter of mode 2, D_{M_2}, μ	1606	1517	1202	1085
Percentage of drops in mode 1	48.9	56.2	53.4	71.5
Percentage of mass in mode 1	1.3	2.0	4.0	7.4
Volume-number-mean diameter of complete distribution, D_{30}, μ	748	666	609	445
Mass-median diameter of complete distribution, D_T, μ	1920	1530	963	850

TABLE II. - Continued. DROP COUNTS OBTAINED WITH PARTICLE ANALYZER AND PROPERTIES OF DROP-SIZE DISTRIBUTIONS

(d) Jet angle, 60°; jet velocity, 60 feet per second; downstream distance, 8 inches

Experimental drop counts					
Average diameter of size group, D_{av}, μ	Velocity difference, Δv, ft/sec				
	-30	0	30	60	120
	Number of drops, ΔN				
242	7098	6646	5628	7459	9727
341	4779	4468	4172	4727	4984
484	3299	3170	2993	3063	2726
682	2617	2332	2330	2298	1590
965	1214	1053	1040	1102	637
1365	507	411	474	393	234
1930	173	118	139	110	54
2720	30	17	30	14	9
3860	3	0	1	1	0
Total	19,720	18,215	16,807	19,167	19,961
Properties of distributions					
Number-median diameter of mode 1, D_{N_1}, μ	180	190	170	200	160
Mass-median diameter of mode 1, D_{M_1}, μ	298	279	293	312	275
Number-median diameter of mode 2, D_{N_2}, μ	460	440	440	520	390
Mass-median diameter of mode 2, D_{M_2}, μ	1290	1153	1306	1145	1074
Percentage of drops in mode 1	62.4	57.4	57.9	68.7	79.6
Percentage of mass in mode 1	4.5	4.4	3.5	6.9	11.9
Volume-number-mean diameter of complete distribution, D_{30}, μ	564	544	575	537	397
Mass-median diameter of complete distribution, D_T, μ	1060	950	1045	925	800

TABLE II. - Continued. DROP COUNTS OBTAINED WITH PARTICLE ANALYZER AND PROPERTIES OF DROP-SIZE DISTRIBUTIONS

(e) Jet angle, 60°; jet velocity, 74 feet per second; downstream distance, 8 inches

Experimental drop counts				
Average diameter of size group, D_{av}, μ	Velocity difference, Δv, ft/sec			
	0	30	60	120
	Number of drops, ΔN			
242	5830	5334	9414	12696
341	4270	4440	5786	7234
484	2876	3035	3518	4332
682	2014	2179	2535	2921
965	846	902	1200	1202
1365	225	237	422	317
1930	32	46	99	76
2720	2	1	11	9
3860	0	0	0	0
Total	16,095	16,174	22,985	28,787
Properties of distributions				
Number-median diameter of mode 1, D_{N_1}, μ	200	230	180	180
Mass-median diameter of mode 1, D_{M_1}, μ	308	371	302	374
Number-median diameter of mode 2, D_{N_2}, μ	500	560	500	500
Mass-median diameter of mode 2, D_{M_2}, μ	916	922	1083	1044
Percentage of drops in mode 1	66.9	68.4	75.5	80.7
Percentage of mass in mode 1	9.1	12.7	9.0	13.6
Volume-number-mean diameter of complete distribution, D_{30}, μ	483	512	475	438
Mass-median diameter of complete distribution, D_T, μ	740	754	865	760

TABLE II. - Concluded. DROP COUNTS OBTAINED WITH PARTICLE ANALYZER AND PROPERTIES OF DROP-SIZE DISTRIBUTIONS

(f) Jet angle, 90°; jet velocity, 30 feet per second; downstream distance, 8 inches

Experimental drop counts			
Average diameter of size group, D_{av}, μ	Velocity difference, Δv, ft/sec		
	37	60	120
	Number of drops, ΔN		
242	4344	4190	8761
341	2764	3138	4784
484	1796	2110	2624
682	1423	1697	1595
965	681	817	548
1365	205	254	135
1930	54	41	14
2720	3	1	2
3860	0	0	0
Total	11,270	12,248	18,463
Properties of distributions			
Number-median diameter of mode 1, D_{N_1}, μ	195	230	180
Mass-median diameter of mode 1, D_{M_1}, μ	315	353	274
Number-median diameter of mode 2, D_{N_2}, μ	550	600	400
Mass-mean diameter of mode 2, D_{M_2}, μ	1025	961	860
Percentage of drops in mode 1	73.7	69.6	74.6
Percentage of mass in mode 1	9.2	10.8	13.9
Volume-number-median diameter of complete distribution, D_{30}, μ	497	530	390
Mass-median diameter of complete distribution, D_T, μ	840	812	640

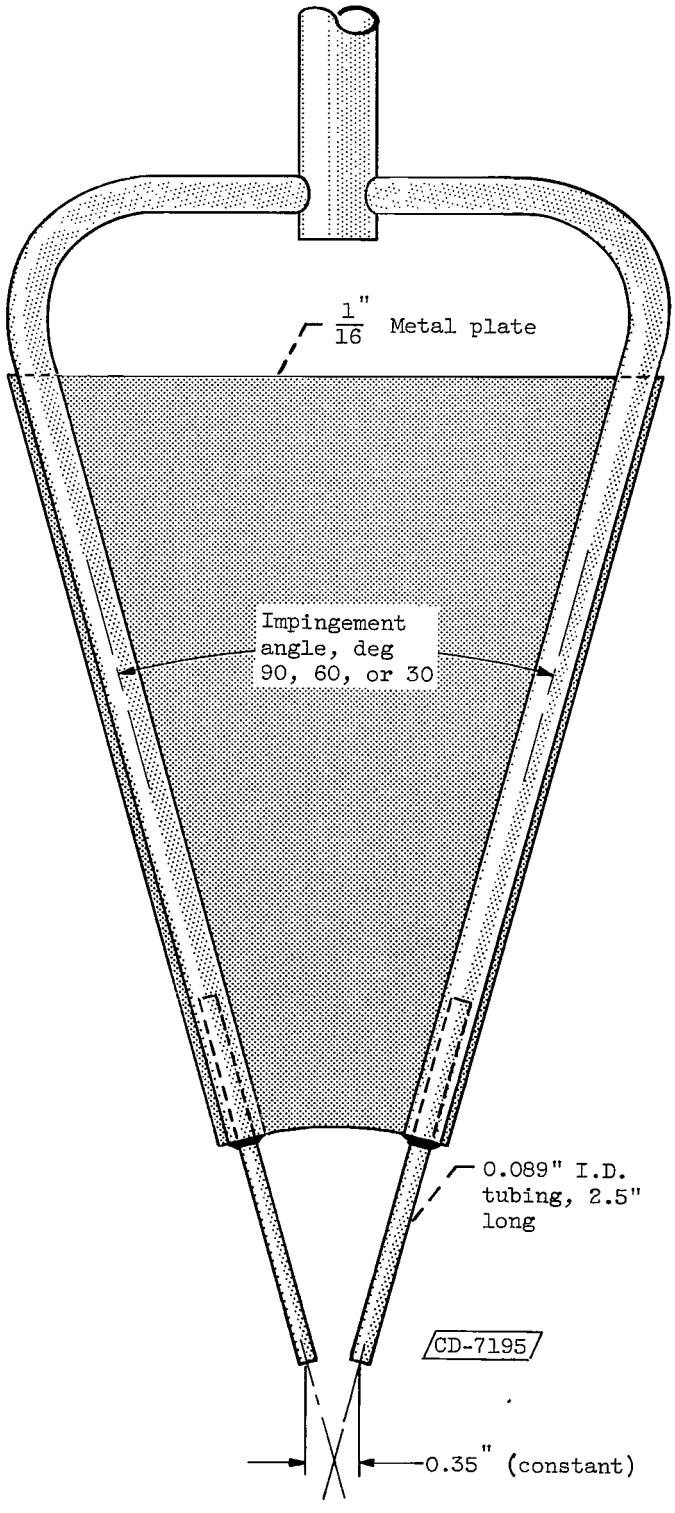

Figure 1. - Impinging-jet injector.

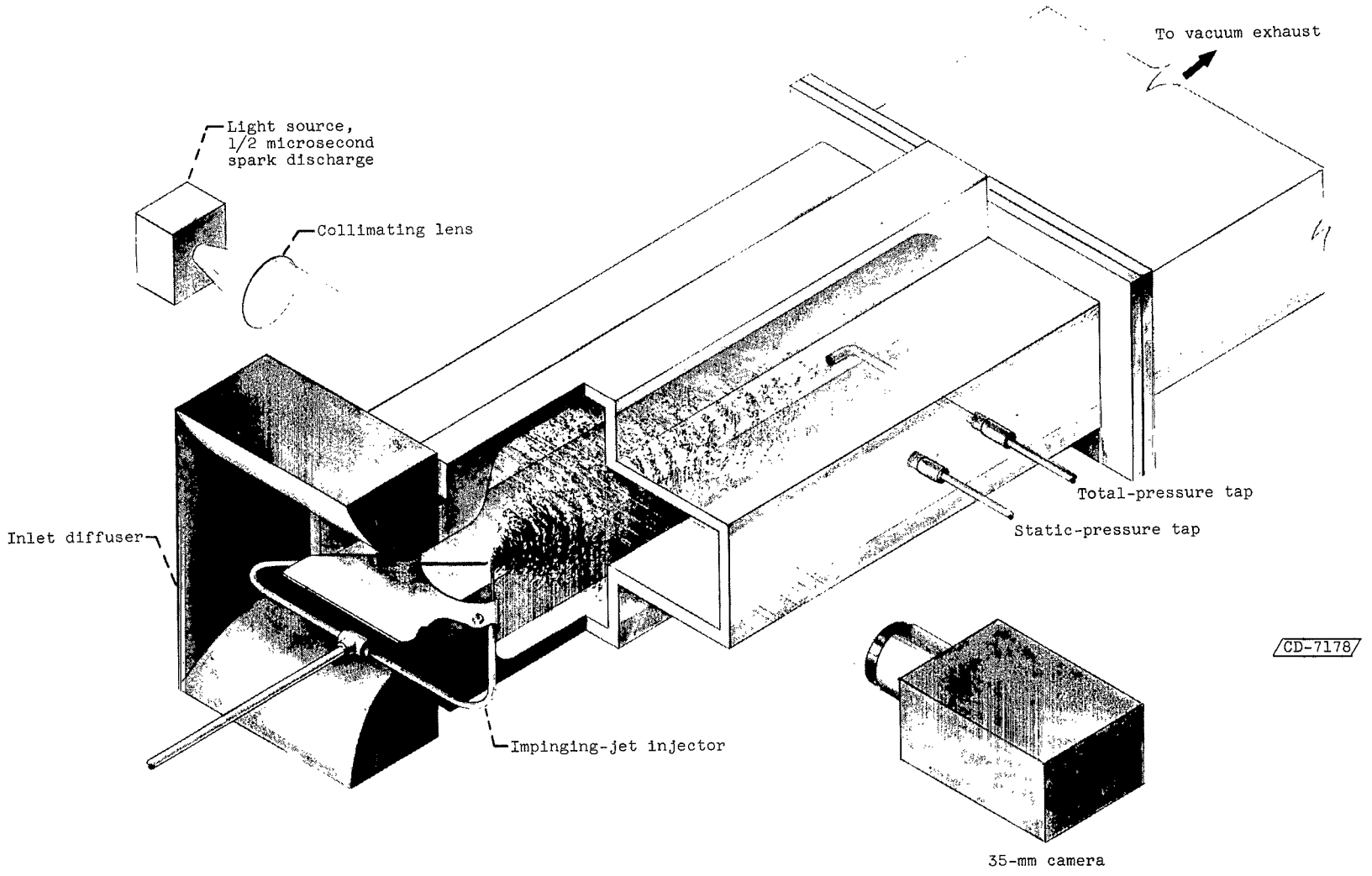

(a) Complete apparatus.

Figure 2. - Experimental apparatus used for drop photographs in air duct.

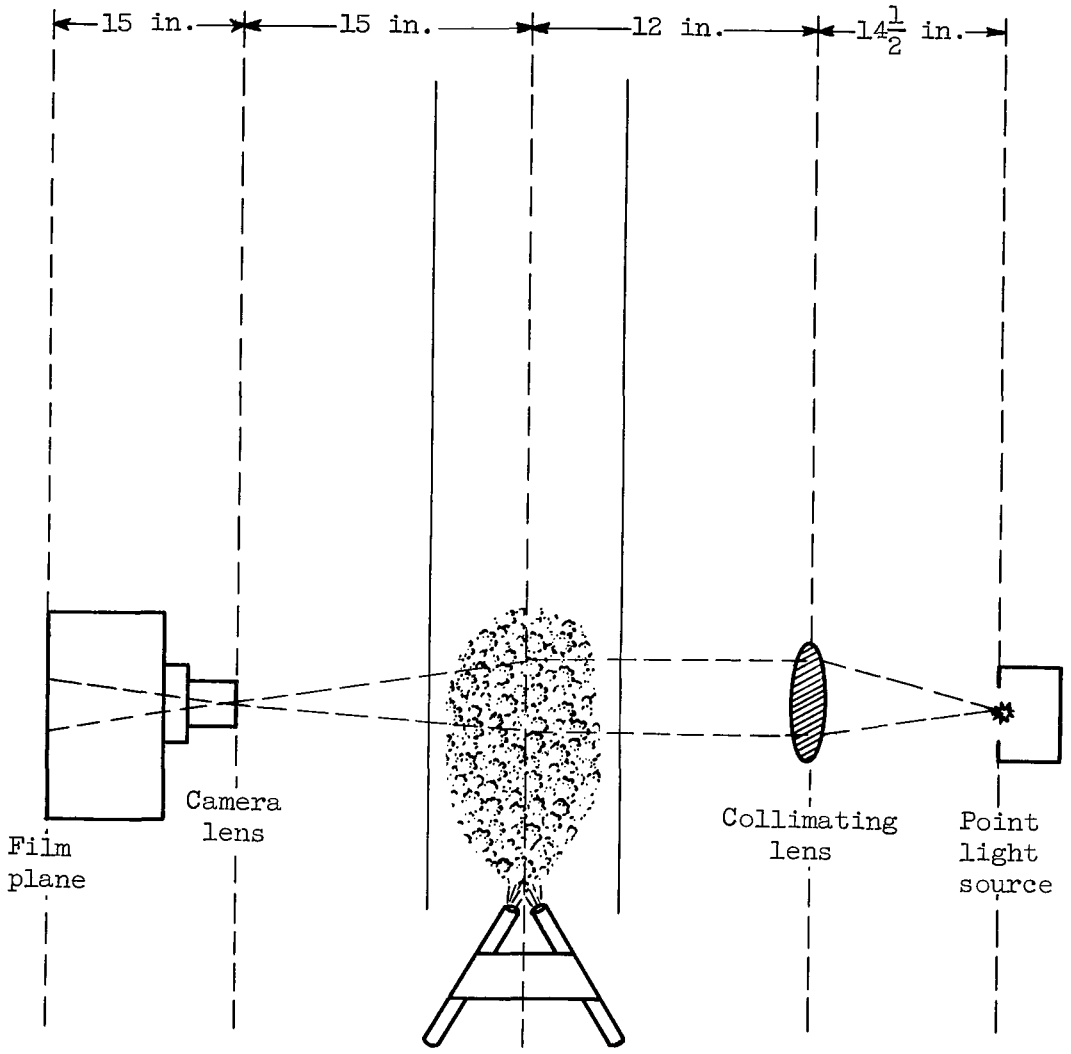

(b) Schematic diagram of optical system.

Figure 2. - Concluded. Experimental apparatus used for drop photographs in air duct.

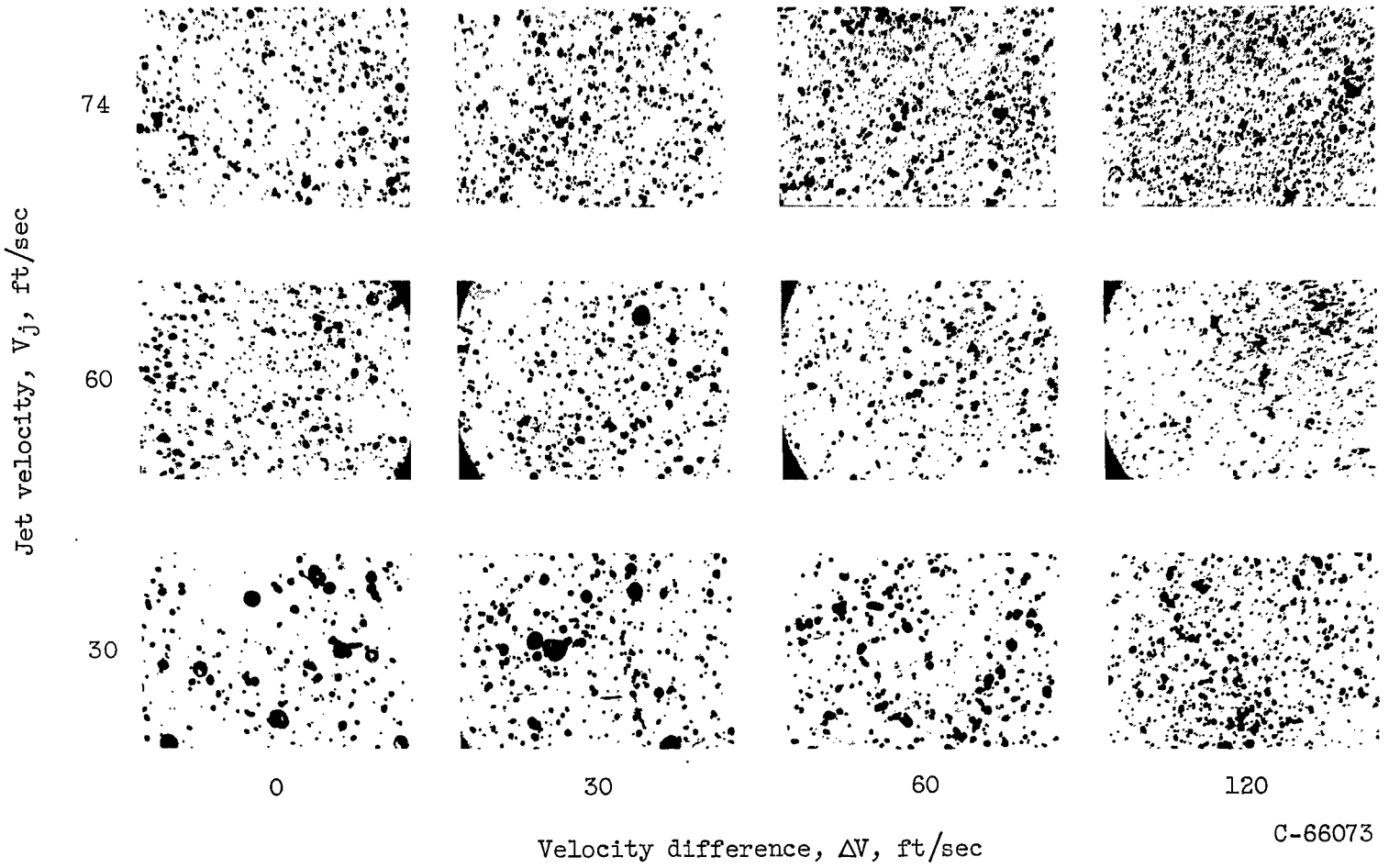

(a) Injector angle, 60°; downstream distance, 8 inches.

Figure 3. - Typical photographs of drop-size distributions.

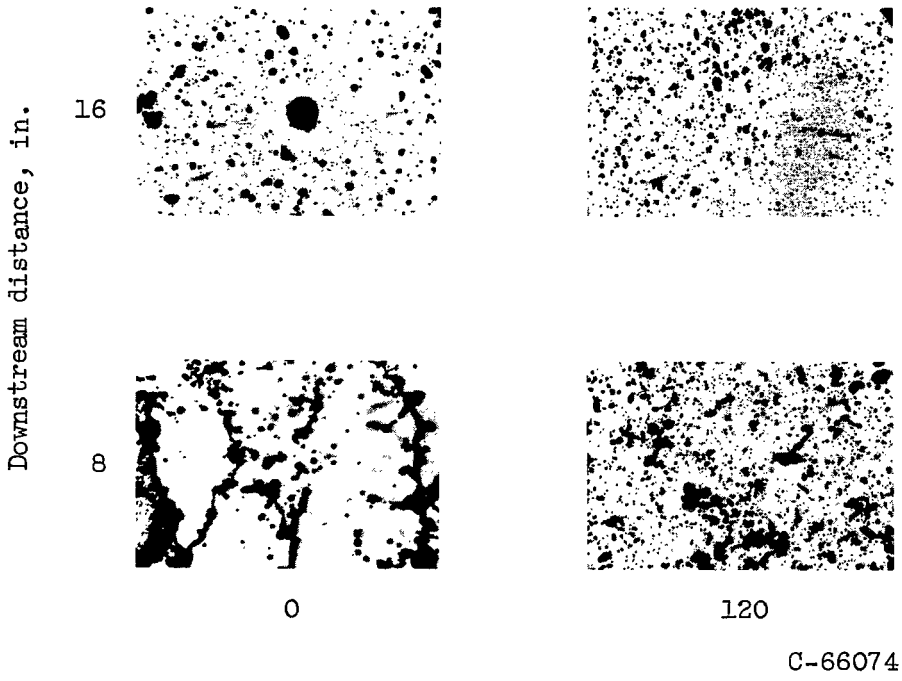

(b) Injector angle, 30°; jet velocity, 74 feet per second.

Figure 3. - Concluded. Typical photographs of drop-size distributions.

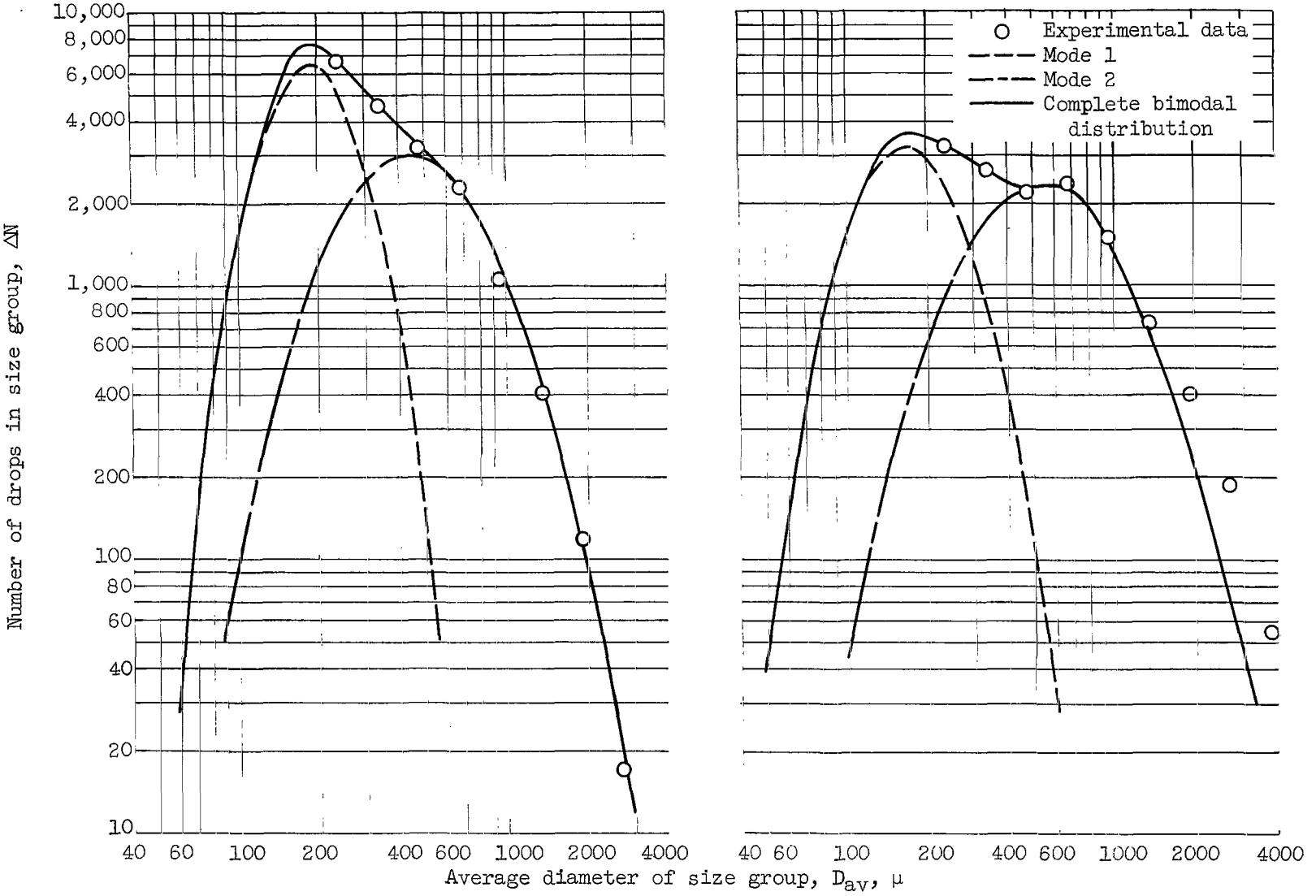

(a) Jet velocity, 60 feet per second.

(b) Jet velocity, 30 feet per second.

Figure 4. - Typical drop-size distributions. Jet angle, 60°; velocity difference, 0 feet per second.

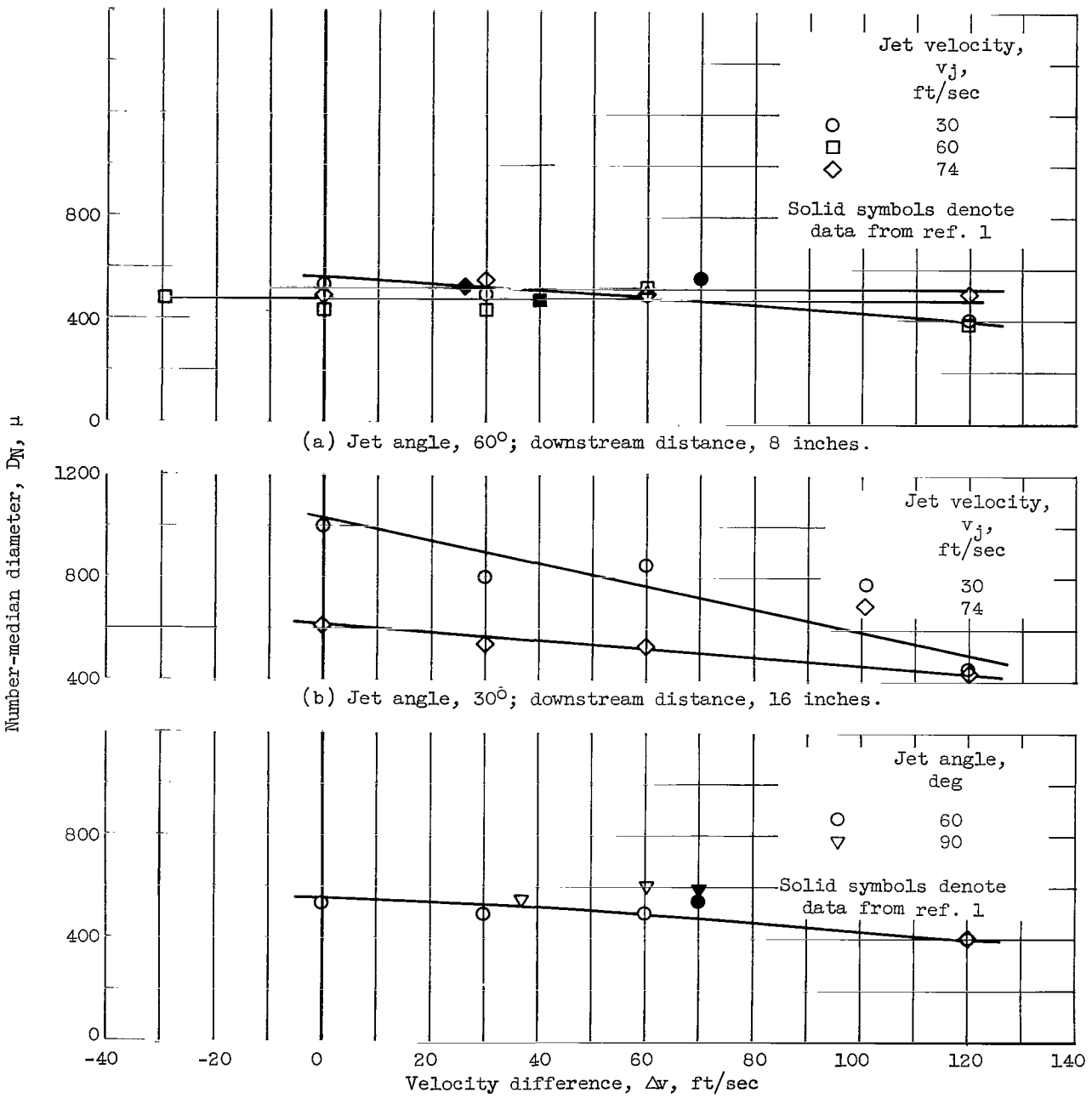

(c) Jet velocity, 30 feet per second; downstream distance, 8 inches.

Figure 5. - Effect of velocity difference on number-median diameter of mode 2.

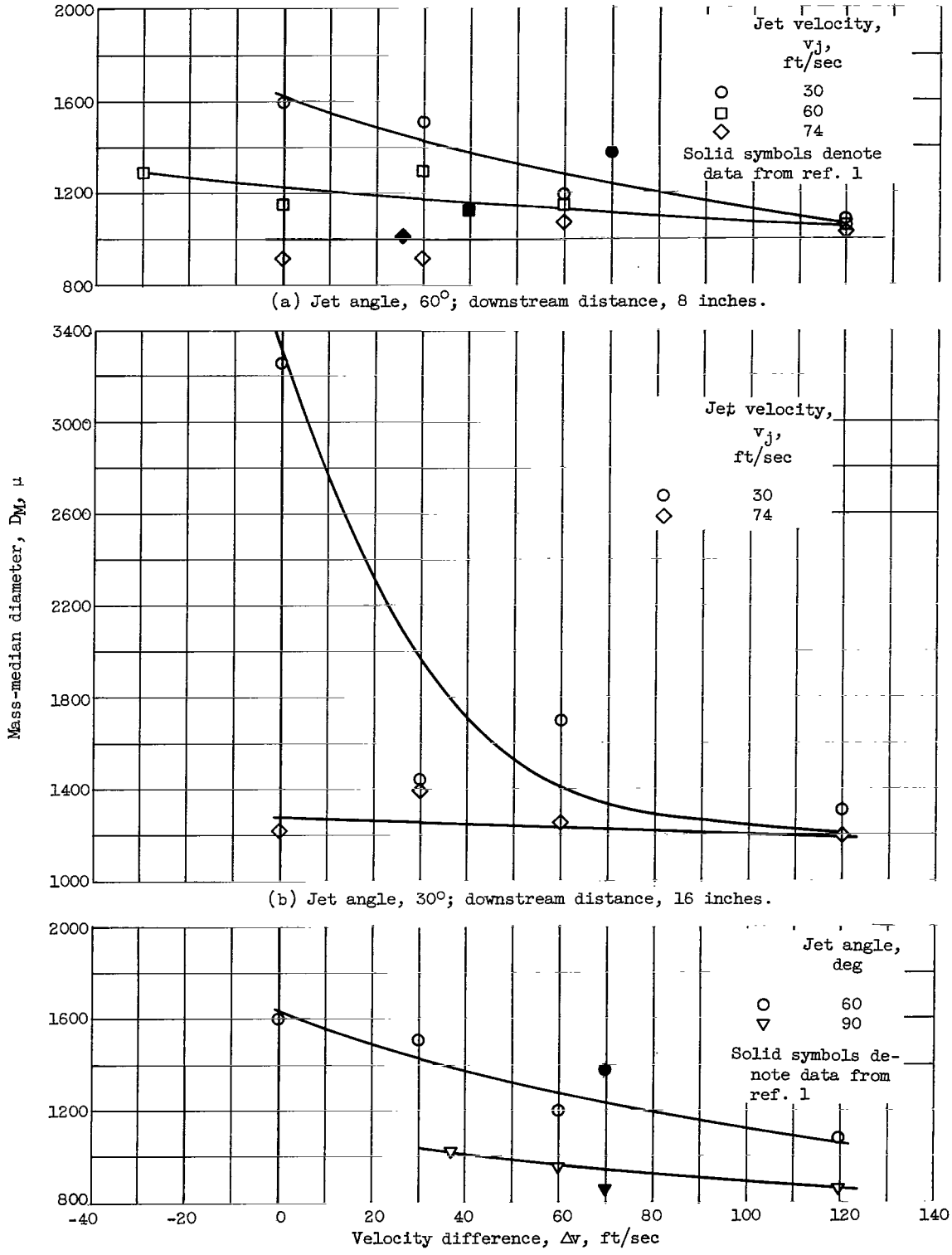

(a) Jet angle, 60°; downstream distance, 8 inches.

(b) Jet angle, 30°; downstream distance, 16 inches.

(c) Jet velocity, 30 feet per second; downstream distance, 8 inches.

Figure 6. - Effect of velocity difference on mass-median diameter of mode 2.

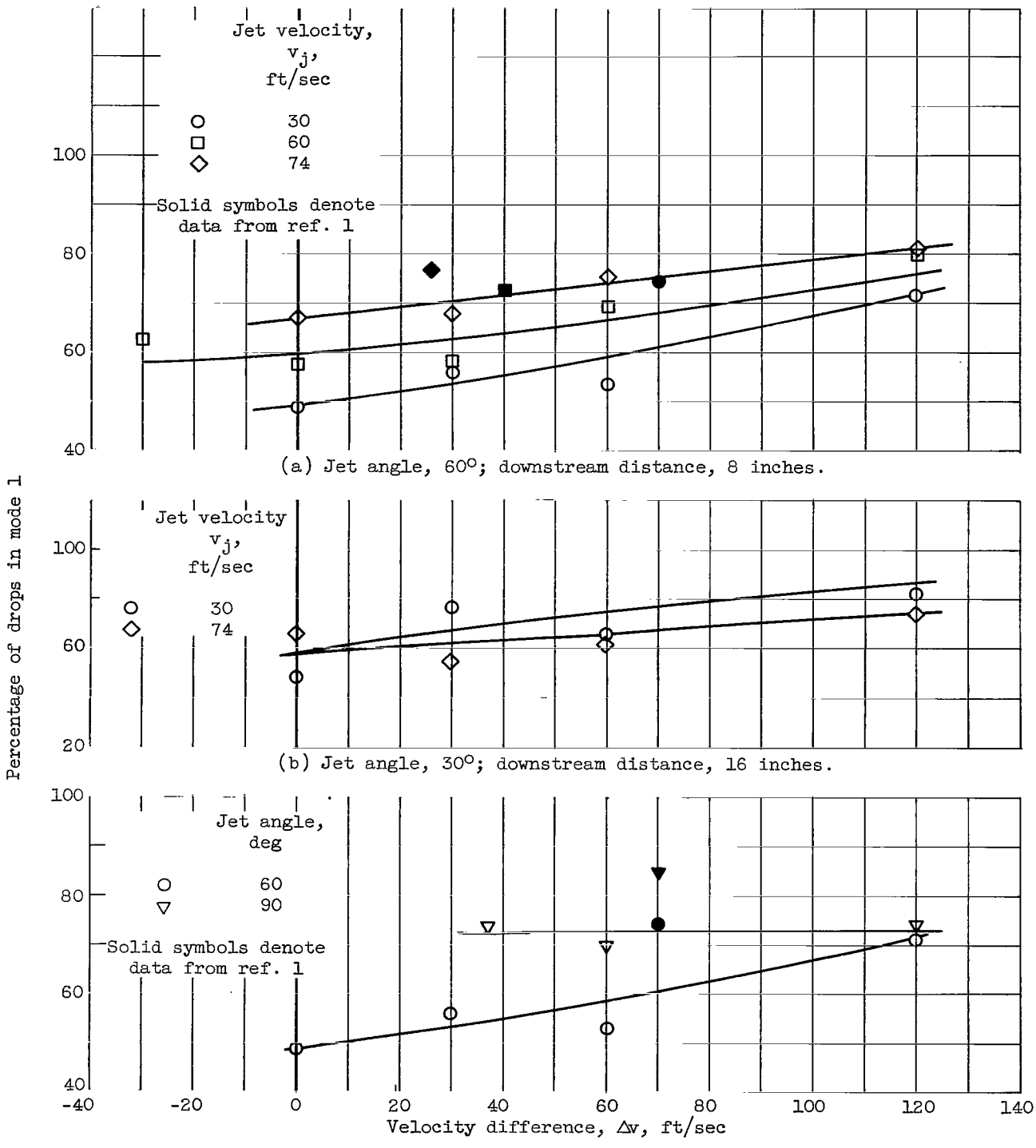

(c) Jet velocity, 30 feet per second; downstream distance, 8 inches.

Figure 7. - Effect of velocity difference on percentage of drops in mode 1.

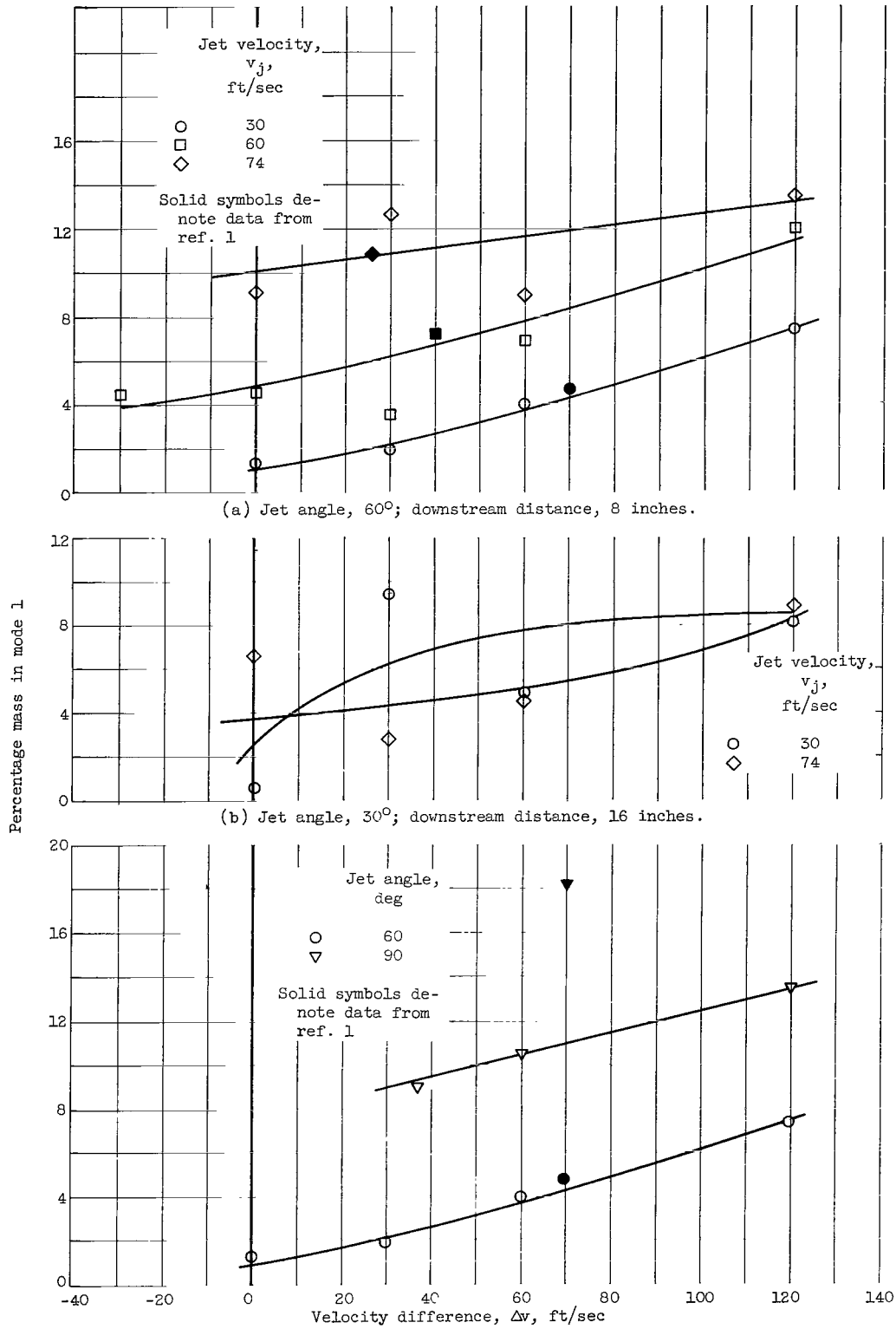

Figure 8. - Effect of velocity difference on percentage of mass in mode 1.

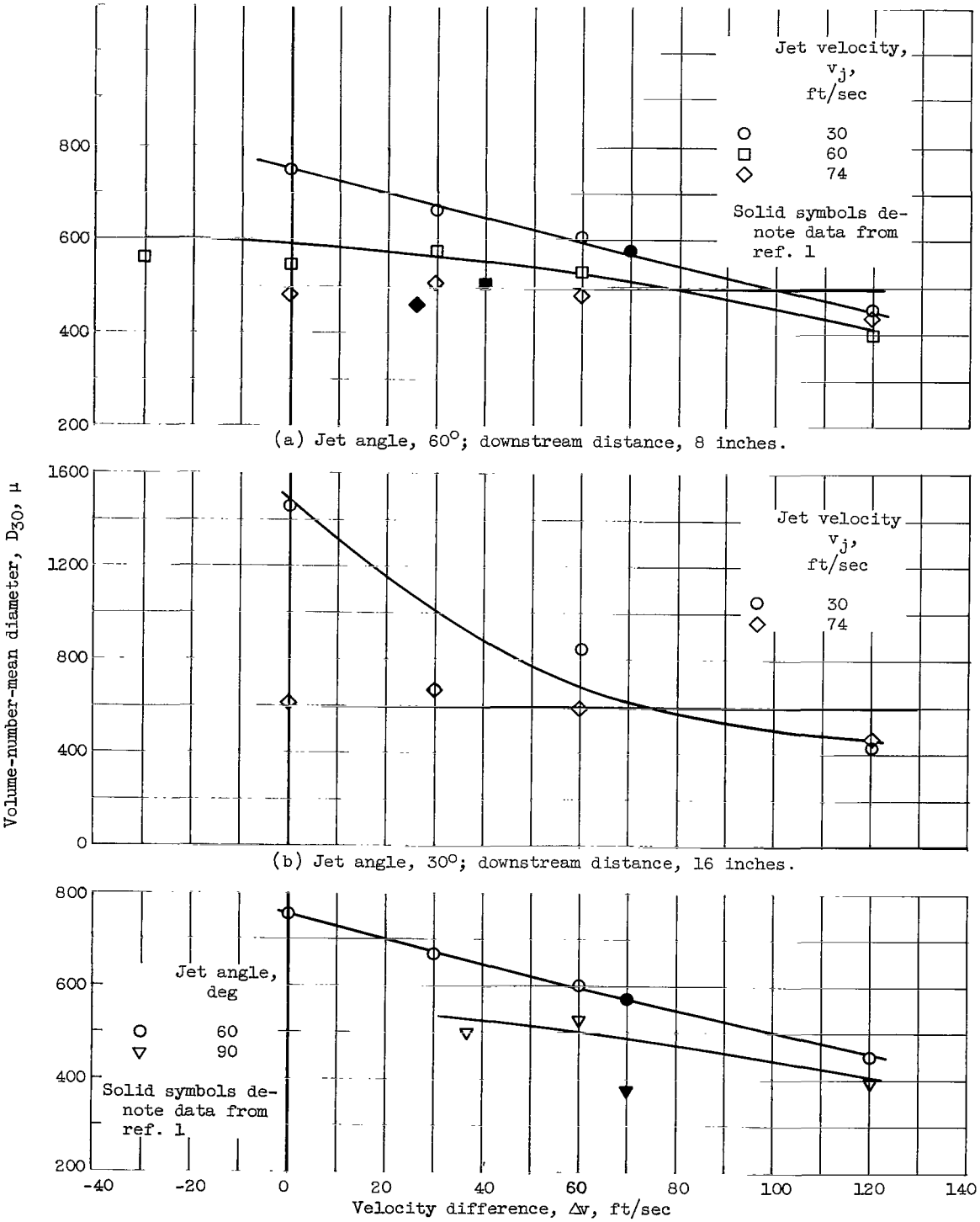

Figure 9. - Effect of velocity difference on volume-number-mean diameter of complete spray distribution.

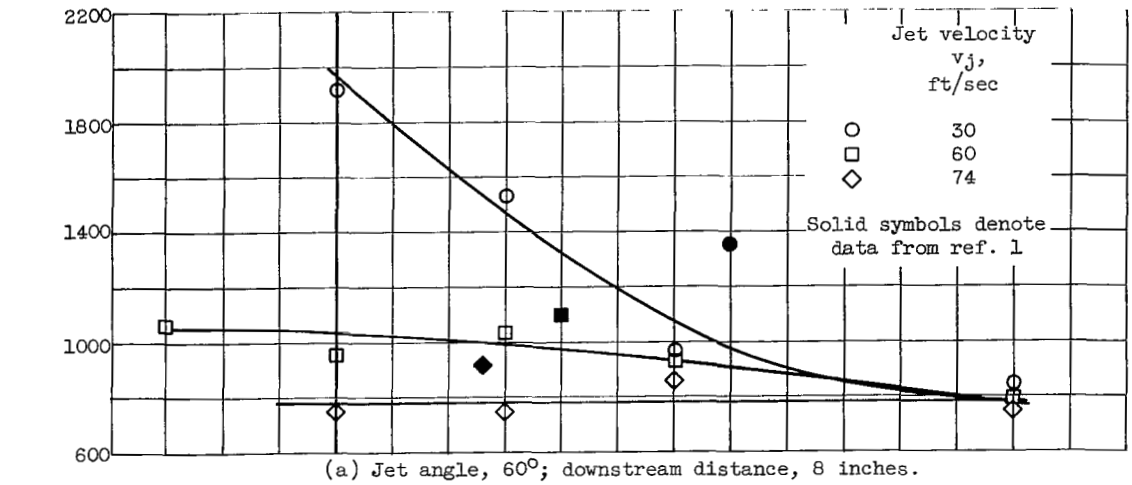

(a) Jet angle, 60°; downstream distance, 8 inches.

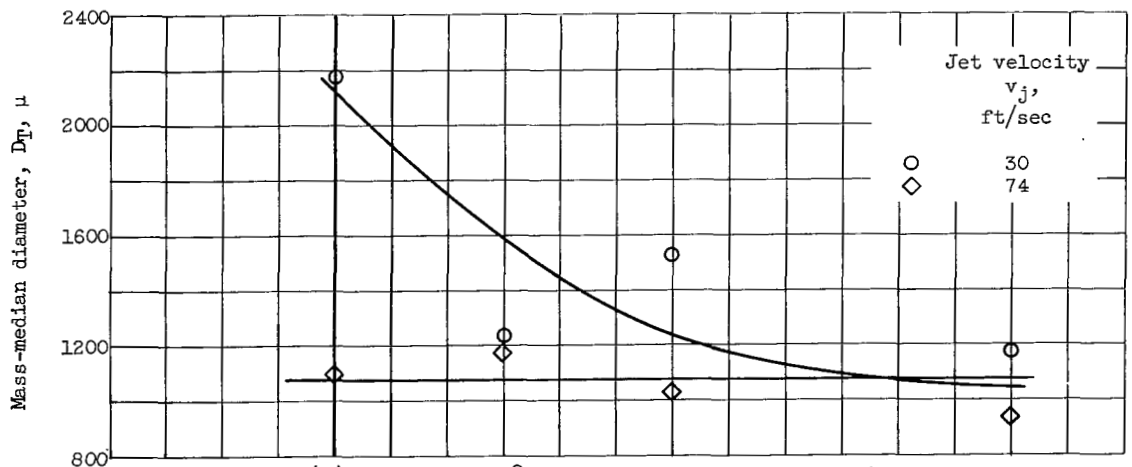

(b) Jet angle, 30°; downstream distance, 16 inches.

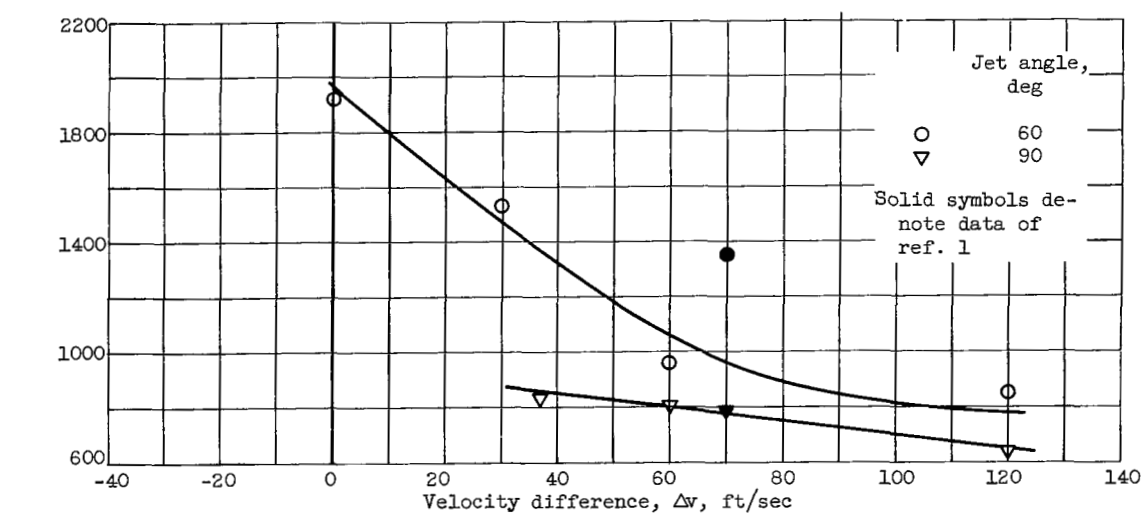

Mass-median diameter, D_m, μ

(c) Jet velocity, 30 feet per second; downstream distance, 8 inches.

Figure 10. - Effect of velocity difference on mass-median diameter of complete distribution.